Decoding Provenance and Tectonothermal Events by Detrital Zircon Fission-Track and U-Pb Double Dating: A Case of the Southern Ordos Basin

ZHANG Shaohua[1], LIU Chiyang[1, *], YANG Minghui[2], WANG Jianqiang[1], BAI Jianke[1, 3] and Huang Hexin[1]

[1] *State Key Laboratory of Continental Dynamics, Department of Geology, Northwest University, Xi'an 710069, Shaanxi, China*
[2] *State Key Laboratory of Petroleum Resource and Prospecting, College of Geosciences, China University of Petroleum, Beijing 102200, China*
[3] *Research Center of Orogenic Geology, Xi'an Center of Geological Survey, China Geological Survey, Xi'an 710054, Shaanxi, China*

Abstract: Multi-dating on the same detrital grains allows for determining multiple different geo-thermochronological ages simultaneously and thus could provide more details about regional tectonics. In this paper, we carried out detrital zircon fission-track and U-Pb double dating on the Permian-Middle Triassic sediments from the southern Ordos Basin to decipher the tectonic information archived in the sediments of intracratonic basins. The detrital zircon U-Pb ages and fission-track ages, together with lag time analyses, indicate that the Permian-Middle Triassic sediments in the southern Ordos Basin are characterized by multiple provenances. The crystalline basement of the North China Craton (NCC) and recycled materials from pre-Permian sediments that were ultimately sourced from the basement of the NCC are the primary provenance, while the Permian magmatites in the northern margin of NCC and Early Paleozoic crystalline rocks in Qinling Orogenic Collage act as minor provenance. In addition, the detrital zircon fission-track age peaks reveal four major tectonothermal events, including the Late Triassic-Early Jurassic post-depositional tectonothermal event and three other tectonothermal events associated with source terrains. The Late Triassic-Early Jurassic (225–179 Ma) tectonothermal event was closely related to the upwelling of deep material and energy beneath the southwestern Ordos Basin due to the coeval northward subduction of the Yangze Block and the following collision of the Yangze Block and the NCC. The Mid-Late Permian (275–263 Ma) tectonothermal event was associated with coeval denudation in the northern part of the NCC and North Qinling terrane, resulting from the subduction of the Paleo-Asian Ocean and Tethys Ocean toward the NCC. The Late Devonian-early Late Carboniferous (348±33 Ma) tectonothermal event corresponded the long-term denudation in the hinterland and periphery of the NCC because of the arc-continent collisions in the northern and southern margins of the NCC. The Late Neoproterozoic (813–565 Ma) tectonothermal event was associated with formation of the Great Unconformity within the NCC and may be causally related to the Rodinia supercontinent breakup driven by a large-scale mantle upwelling.

Key words: provenance, multiple tectonothermal events, detrital zircon double dating, Ordos Basin, North China Craton

Citation: Zhang et al., 2019. Decoding Provenance and Tectonothermal Events by Detrital Zircon Fission-Track and U-Pb Double Dating: A Case of the Southern Ordos Basin. Acta Geologica Sinica (English Edition), 93(4): 845–856. DOI: 10.1111/1755-6724.13802

1 Introduction

Detrital mineral geochronology and thermochronology are increasingly employed to determine the timing of crystallization and multiple tectonothermal events, with relevance for sediment provenance and tectonic processes (Fedo et al., 2003; Hodges et al., 2005; Reiners et al., 2005; Carrapa, 2010; Hietpas et al., 2010; Filleaudeau et al., 2012; Lawton, 2014; Mark et al., 2016; Zhao et al., 2016; Cheng et al., 2016; Glorie et al., 2017; Zhang et al., 2018a). Detrital zircon U-Pb geochronology is the popular approach to extracting such information because zircon has a very high closure temperature during weathering, erosion, deposition, and burial in the sedimentary environment so that it could record the age of the igneous rock from which it was originally derived (Fedo et al., 2003; Dickinson and Gehrels, 2009; Thomas, 2011; Cawood et al., 2012; Gehrels, 2014). Unfortunately, the refractory nature of the U-Pb zircon system implies that it is hard to record low- to medium-temperature tectonothermal events during denudation and multiple erosion-deposition cycles (Carrapa, 2010; Thomas, 2011). During the last two decades breakthroughs in multi-dating on the same detrital grains allow for determining multiple different geo-thermochronological ages simultaneously, which could provide more details about sediment provenance and regional tectonic processes (Carter and Moss et al., 1999; Carter and Bristow, 2000; Bernet et al.,

* Corresponding author. E-mail: lcy@nwu.edu.cn

2006; Dias et al., 2011, 2018; Shen et al., 2012, 2016; Cao et al., 2015; De Grave et al., 2016; Glorie and De Grave, 2016; Thomson et al., 2017; Xu et al., 2017). Detrital zircon fission-track and U-Pb double dating represents a particularly effective thermo- and geochronometer combination, given that the low (240±30°C) and high (>700° C) temperature sensitivity windows of these systems and the abundance of zircon as an accessory mineral in many igneous, metamorphic, and sedimentary rocks (Carter and Bristow, 2000; Bernet and Garver, 2005; Bernet et al., 2006; Carrapa, 2010). Detrital zircon fission-track and U-Pb double dating has been proven as a robust method to unravel regional tectonics by integrated analysis of double-dated single zircon grains from each sample (Bernet et al., 2006; Dias et al., 2011, 2018; Curvo et al., 2013; Cao et al., 2015).

The Ordos Basin of the western North China Craton is a multi-cycle superimposed basin (Yang et al., 2005; Liu et al., 2008; Zhu et al., 2013). During the Late Paleozoic to Middle Triassic, the Ordos Basin was an intracratonic basin with tectonically active margins (Yang et al., 2005, 2015; Liu et al., 2008; Zhu et al., 2013). Although the tectonic activity of majority intracratonic basins is quite weak (Klein and Hsui, 1987; Allen and Armitage, 2012; Pinet et al., 2013), the sediments within intracratonic basins derived from distant tectonically active margins could chronicle long-term crustal evolution of the source terrains, erosion-transport-deposition processes, and post-depositional tectonothermal events, offering invaluable information about regional tectonic evolution (Cawood et al., 2007; Kounov et al., 2013; Guadagnin et al., 2015; Dias et al., 2018). However, little attention has been paid to unravel the tectonic information archived in the sediments of intracratonic basins. The main purpose of this study is to utilize integrated detrital zircon fission-track and U-Pb double dating on the Late Paleozoic to Middle Triassic sediments of the southern Ordos Basin, to decipher the long-term crustal evolution of the source terrains and discern hidden regional tectonothermal events.

2 Geological Setting

The North China Craton (NCC), or the North China Plate, can be divided into the Eastern and Western Blocks by the Trans-North China Orogen that represents the collision of the two blocks at approximately 1.85 Ga (Zhao et al., 2001), which suffered later reformation (Kusky et al., 2007). The Ordos Basin in the western block of the NCC, surrounded by the Qinling Orogenic Collage in the south, the Yinshan-Yanshan tectonic belt in the north, the Lvliang Mountain in the east, the Qilian Orogenic Collage in the southwest (Fig. 1), is a large intraplate basin with multi-stage evolutionary history (Yang et al., 2005, 2015; Liu et al., 2008).

After the finial cratonization of the NCC at approximately 1.82 Ga (Zhai, 2011, 2014; Liu et al., 2012), the Ordos area began to develop sedimentary cover (Lu et al., 2008). The Meso-Neoproterozoic volcaniclastic and carbonate sediments are the first sedimentary cover in the Ordos area during intracontinental rifting and aulacogen development period (Zhai et al., 2014; Chen et al., 2016; Gong et al., 2016). Subsequently, the Ordos area experienced a long-term denudation (He et al., 2017) and then stepped into a cratonic evolutionary stage during the latest Neoproterozoic-Early Paleozoic (Yang et al., 2005; Bai et al., 2013). During the Middle Ordovician-Early Carboniferous, the Ordos area experienced a long-term of uplift and denudation again, resulting ~130 m.y. of missing geologic record (Yang et al., 2005; Wang et al., 2006). Then, it subsided and evolved as an intracratonic basin during the Late Paleozoic to Middle Triassic (Yang et al., 2015). During latest Middle Triassic to Late Triassic, tectonic differentiation of the NCC occurred initially, as evidenced by the denudation of the eastern NCC and the rapid subsidence of the Ordos Basin (Liu et al., 2008; Zhao et al., 2009), which might be a respond to the coeval collision along the Mianlue Suture that finally combinated the South Qinling, the South China plate, and the NCC (Meng and Zhang, 2000; Meng, 2017). After the latest Triassic-Early Jurassic uplift (Zhang et al., 2018b), tectonic differentiation of the NCC further strengthened and the Middle Jurassic-Early Cretaceous subsidence of Ordos Basin was interrupted by a transient tectonic uplift event at the Late Jurassic (Liu et al., 2008; Zhang et al., 2011; Yang et al., 2015). Later, the convergence of the Pacific Ocean Plate and the Indian-Australian Plate toward the Eurasia Plate further complicated the Ordos Basin, and as such most of this region lacks Late Cretaceous-early Miocene sediments, except for the western part (Li and Li, 2008). Accompanying with the outward-growth of Tibetan Plateau and the central Asian aridification (Guo et al., 2004; Wang et al., 2014), the Ordos area successively deposited the late Miocene-Pliocene Red Clay sequence and the Quaternary loess-paleosol sequence, constituting the so-called Chinese Loess Plateau (Sun et al., 2006).

3 Samples and Methodology

In this study, seven Permian-Middle Triassic sandstone samples (Table 1; Fig. 2), 3 kg each, were collected from the outcrops in the southern Ordos Basin. Enough zircon grains for ZFT test were successfully separated from all of the seven samples, using standard heavy liquid and magnetic separation techniques.

ZFT analysis was performed in the ChronusCamp Research, Brazil. The method applied is based on a direct uranium determination through LA-ICP-MS (Hasebe et al., 2004; Soares et al., 2014). Such method also allows to determine the U-Pb ages simultaneously. Experimental procedures for this method are described briefly below.

Firstly, zircon grains per sample were incrusted in Teflon PFA with a thermal plate. Subsequently, sandpapers with grit sizes of #1200, #2400 and #4000 were used to grind the zircons, followed by a polishing using diamond paste with particle size of 1/4 μm. Then samples were etched using an eutectic solution (KOH : NaOH, 1:1) at 220°C for 12 h to reveal spontaneous zircon fission tracks. Zircon fission track density was analyzed under an optical microscope (Leica DM 6000M). The uranium concentration and U-Pb age were carried out with the Agilent 7700 quadrupole ICP-MS coupled with UP213

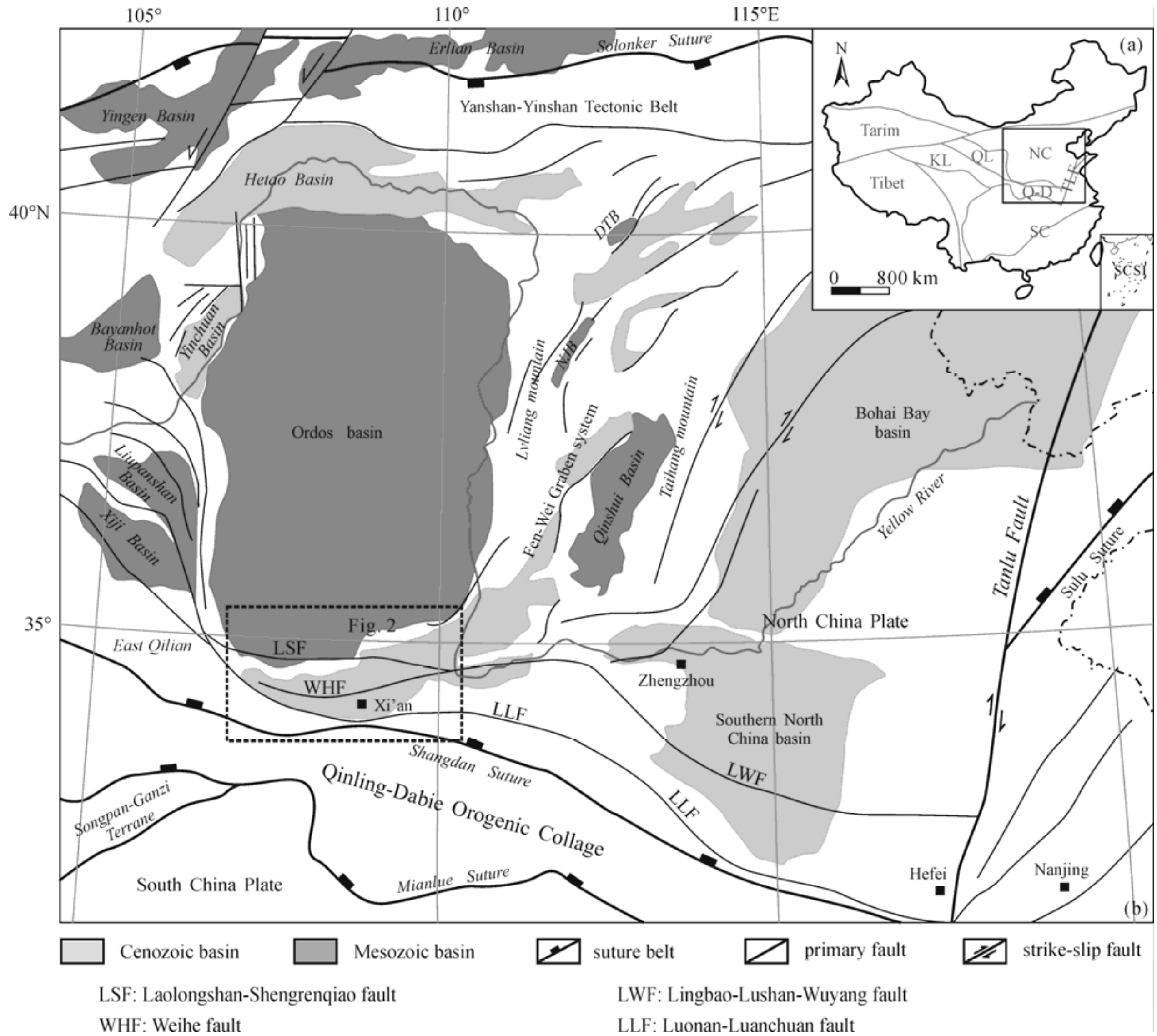

Fig. 1. Regional tectonics and Mesozoic-Cenozoic basins distribution of the North China Plate and its adjacent regions (modified from Darby and Ritts, 2002).

KL, Kunlun orogenic collage; NC, North China; Q-D, Qinling-Dabie orogenic collage; QL, Qilian orogenic collage; SC, South China; TLF, Tancheng-Lujiang Fault; NJB, Ningwu-Jingle basin; DTB, Datong basin.

Table 1 Sample information for zircon fission-track and U/Pb double dating in southern Ordos basin

Sample ID	Lithology	Strata	Longitude (E)	Latitude (N)	Elevation (m)
WB2	Sandstone	Middle Triassic	107°46′05″	34°38′58″	1113
WB3	Sandstone	Lower Permian	108°29′58″	34°38′48″	941
WB4	Sandstone	Lower Triassic	108°40′59″	34°44′38″	674
WB5	Sandstone	Upper Permian	108°41′29″	34°44′11″	652
WB6	Sandstone	Lower Permian	108°41′31″	34°44′07″	649
WB7	Sandstone	Lower Permian	110°29′55″	35°36′38″	767
WB9	Sandstone	Lower Permian	109°10′36″	35°01′36″	1314

NewWave laser ablation. The spot size was chosen to cover the maximum area which fission tracks were measured. The LA-ICP-MS calibration was carried out using Fish Canyon Tuff as age standard sample. Moreover, NIST610 standard glass was used to control the LA-ICP-MS performance. Finally, the fission-track age was determined following Donelick et al. (2005) equation. Our goal was to date about 100 grains per sample, to achieve the required level of statistical adequacy for provenance studies (Vermeesch, 2004). However, it was not possible to find this number of countable grains in all samples because of inclusions and dislocations.

The Kolmogorov-Smirnov test ($P(\chi^2)$) (Galbraith, 1984) was used to quantify age homogeneity. When $P(\chi^2)$ >5%, ZFT samples contain a single-age population, while $P(\chi^2)$ <5% may reflect a mixture of different age components, the decomposition of the grain age is necessarily required (Gallagher et al., 1998). Many methods were used to decompose a ZFT grain age distribution from sandstone rocks into component grain age populations (Brandon, 1992; Ketcham et al., 2003; Giorgis et al., 2017). In this paper, samples with large scatter in single-grain ZFT ages ($P(\chi^2)$ <5% and/or exhibiting dispersion exceeding 25%), were decomposed with the binomial peak-fitting method using RadialPlotter software (Vermeesch, 2009).

4 Results

4.1 ZFT analysis

The ZFT data set are presented in Table 2. Radial plots and double dating plots of single grain age data distributed in seven samples from the Permian-Middle Triassic sediments are illustrated in Fig. 3.

All samples failed the χ^2 test (P (χ^2) <5%) and are characterized by age dispersions D>35%, which are typical for over-dispersed detrital grain age distributions, indicating a mixture of different grain-age components (Galbraith, 1981; Brandon, 1992). Using binomial peak fitting (Brandon, 1992; Vermeesch, 2009), the detrital ZFT age distributions of each sample were decomposed into two or three distinct age populations (Table 3), which can be grouped in five peak age populations that we term P1 to P5. The youngest age population P1 (WB2: 225±28 Ma, 43% of dated grains; WB5: 179±40 Ma, 40% of dated grains; and WB6: 207±24 Ma, 21% of dated grains) is apparently younger than the corresponding depositional age for some of the samples, implying partial resetting of these samples. The second younger age population P2 (WB3: 263±19 Ma, 70% of dated grains; WB4: 275±19 Ma, 63% of dated grains; and WB9: 269±23 Ma, 54% of dated grains) overlaps the corresponding depositional ages for these samples within error, or is slightly older, implying either syn-depositional volcanic input or rapid exhumation of the source terrains. The rest three older age populations are clearly older than the corresponding depositional ages for these samples, recording exhumation history of the source terrains rather than that of the basin. More detailly, three samples contain a Late Ordovician-earliest Carboniferous age population P3 (WB5: 459±50 Ma, 60% of dated grains; WB6: 368±28 Ma, 52% of dated grains; and WB7: 348±33 Ma, 53% of dated grains), while

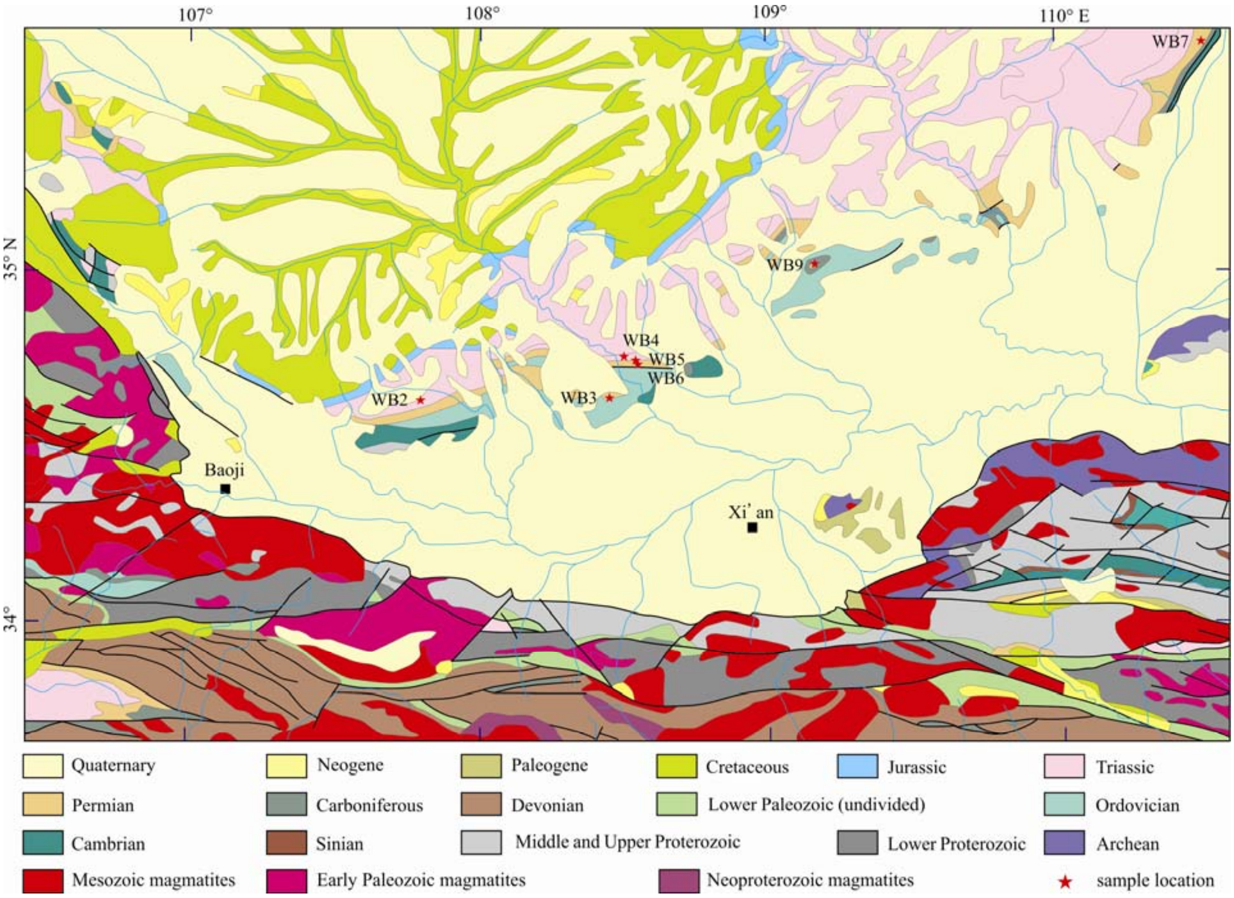

Fig. 2. Simplified geologic map showing sample locations in the southern Ordos Basin.

Table 2 Zircon fission-track results of the Late Paleozoic-Middle Triassic sediments from the southern Ordos Basin

Sample ID	No. of grains	Ns	ρs (107 cm^2)	Pooled ^{238}U (ppm)	P(χ^2) (%)	Dispersion (%)	Mean age (Ma ± 1σ)	Pooled age (Ma ± 1σ)	Central age (Ma ± 1σ)
WB2	17	273	1.61	76	0	55	463.2±30.8	355.3±23.6	391 ± 58
WB3	14	313	2.12	108.6	0	70	539.5±33.9	336.4±21.2	398 ± 78
WB4	20	387	1.98	96	0	50	485.1±27.1	342.2±20.0	396 ± 49
WB5	8	134	1.54	79.4	0	43	329.9±30.0	316.4±28.7	307 ± 55
WB6	14	501	1.85	75.9	0	47	448.9±23.6	347.2±18.2	396 ± 53
WB7	19	485	1.98	72.3	0	39	511.7±27.2	439.0±23.3	465 ± 48
WB9	19	364	1.4	68.7	0	38	422.5±25.0	345.1±20.4	381 ± 39

Note: Ns = number of spontaneous tracks counted; ρs = spontaneous track density.

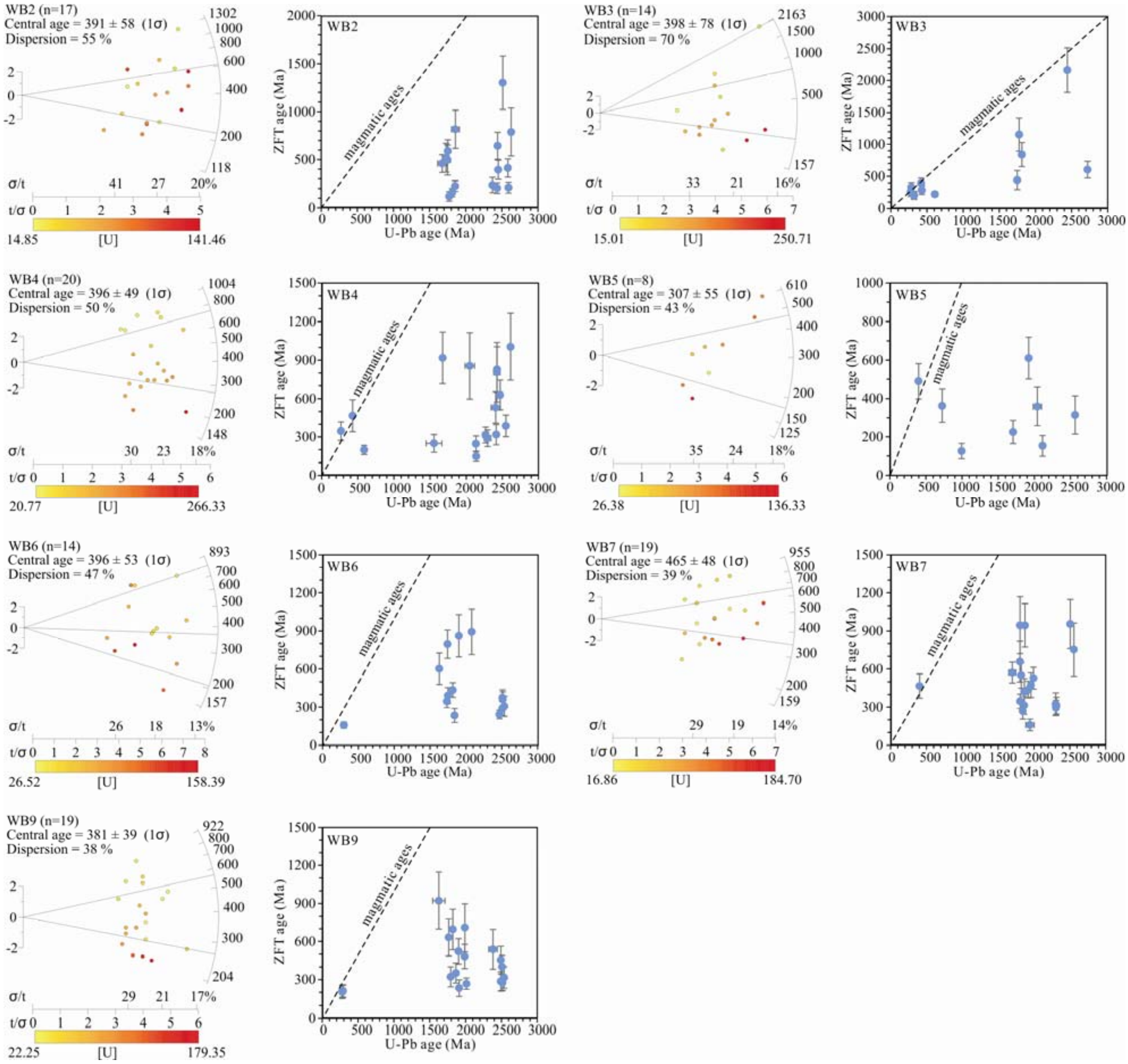

Fig. 3. Radial plots (left) and fission-track versus U-Pb ages for double-dated single zircon grains (right) for each sample in this study.

Table 3 Decomposed peak ages for zircon fission–track data from the southern Ordos Basin

Sample ID	No. of grains	Age range (Ma)	P1 (Ma)	P2 (Ma)	P3 (Ma)	P4 (Ma)	P5 (Ma)
WB2	17	118.1–1301.9	225±28 (43%)			614±52 (57%)	
WB3	14	156.6–2163.4		263±19 (70%)		813±110 (22%)	2146±364 (7%)
WB4	20	148.2–1004.2		275±19 (63%)		739±70 (37%)	
WB5	8	125.5–610.4	179±40 (40%)		459±50 (60%)		
WB6	14	157.4–861.5	207±24 (21%)		368±28 (52%)	794±75 (27%)	
WB7	19	158.8–954.7			348±33 (53%)	656±61 (47%)	
WB9	19	203.8–922.0		269±23 (54%)		565±55 (46%)	

the P3 in samples WB5 and WB6 is vague due to partial resetting; six samples (WB2, WB3, WB4, WB6, WB7, and WB9) contain a Late Neoproterozoic age population P4 (813–565 Ma, 22%–57% of dated grains), similarly, the P4 in samples WB2 and WB6 is vague because of partial resetting; in addition, Sample WB3 generates a minor Paleoproterozoic age population P5 (2146 ± 364 Ma, 7% of dated grains).

4.2 Combined ZFT-U-Pb analysis

As mentioned in the methodology, zircon grains, for which ZFT ages were analyzed, have been conducted with the LA-ICP-MS zircon U-Pb dating. Almost all of the dated zircons have high Th/U values (>0.1), interpreted as being of magmatic origin (Hoskin and Black, 2000). In Fig. 4 it can be observed that most of the dated zircons fall close to the concordia line, implying the ages can be

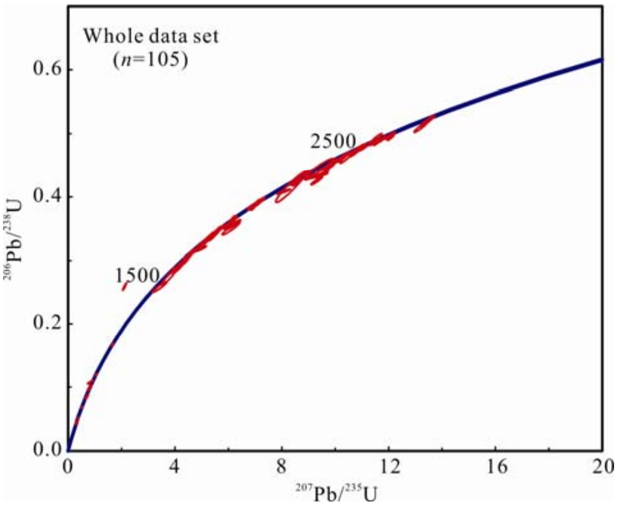

Fig. 4. Concordia plot for U-Pb ages of zircon that were dated with the fission-track-U-Pb double dating method from the Permian-Middle Triassic sediments in the southern Ordos Basin.

regarded as the age of crystallization of the zircons, which could be used to constrain zircon provenance. However, some of the zircons slightly deviate from the concordia line. In the following part, we do not take into account ages that were more than 10% discordant. The peak age populations were identified and calculated using DensityPlotter software (Vermeesch, 2009).

The U-Pb ages of the dated zircons range widely from 2721 to 267 Ma, and can be grouped in five peak age populations (Fig. 5): 2532.9±2.6 Ma (34.2±7%), 1997.5±3.8 Ma (16.4±3.7%), 1767.9±3.5 Ma (32.3±4.6%), 455.3±1.2 Ma (8.6±2.7%), and 290.68±0.78 Ma (8.6±2.7%), seemingly reflecting these sediments derived from multiple provenance areas. Double dating plots (Fig. 5) reveal that most of ZFT ages are significantly younger than their corresponding U-Pb ages and thus reveal cooling related to exhumation of source terrains. Moreover, some zircons generate Permian, Silurian-Devonian and Paleoproterozoic ZFT ages overlapping their U-Pb ages within error and hence might record rapid cooling from crystallization to exhumation in the source areas.

5 Discussions

5.1 Zircon provenance

Detrital zircon U-Pb analysis is a powerful tool for determining the provenance of clastic sediments by matching detrital zircon U-Pb ages with the crystallization ages of potential source rocks (Thomas, 2011; Gehrels, 2014). However, the recycling of detrital zircon through multi-cycle sedimentation may mask some critical information and thus lead to an ambiguous interpretation of provenance (Thomas, 2011). The U-Pb isotopic system closes at temperatures of >700° C in most zircons (Carrapa, 2010), whereas the ZFT have a closure temperature of 240±30°C in natural systems (Bernet and Garver, 2005). Consequently, combined U-Pb and fission-track double dating on single detrital zircon grains could generate complementary crystallization age and thermal evolution information to improve our understanding of the evolution of the source terrains (Carter and Moss, 1999; Carter and Bristow, 2000; Bernet et al., 2006; Shen et al., 2012, 2016; Curvo et al., 2013; Cao et al., 2015; Fosdick et al., 2015; Dias et al., 2018).

From the view of detrital zircon U-Pb geochronology, the five peak age populations reflect the Permian-Middle Triassic sediments in the southern Ordos Basin derived from multiple provenance areas. Specifically, the three prominent Precambrian U-Pb age populations with peaks at 2532.9±2.6 Ma (34.2±7%), 1997.5±3.8 Ma (16.4±3.7%), 1767.9±3.5 Ma (32.3±4.6%), respectively, match well with the typical U-Pb age peaks of the basement of the NCC (Zhai and Liu, 2003; Zhao et al.,

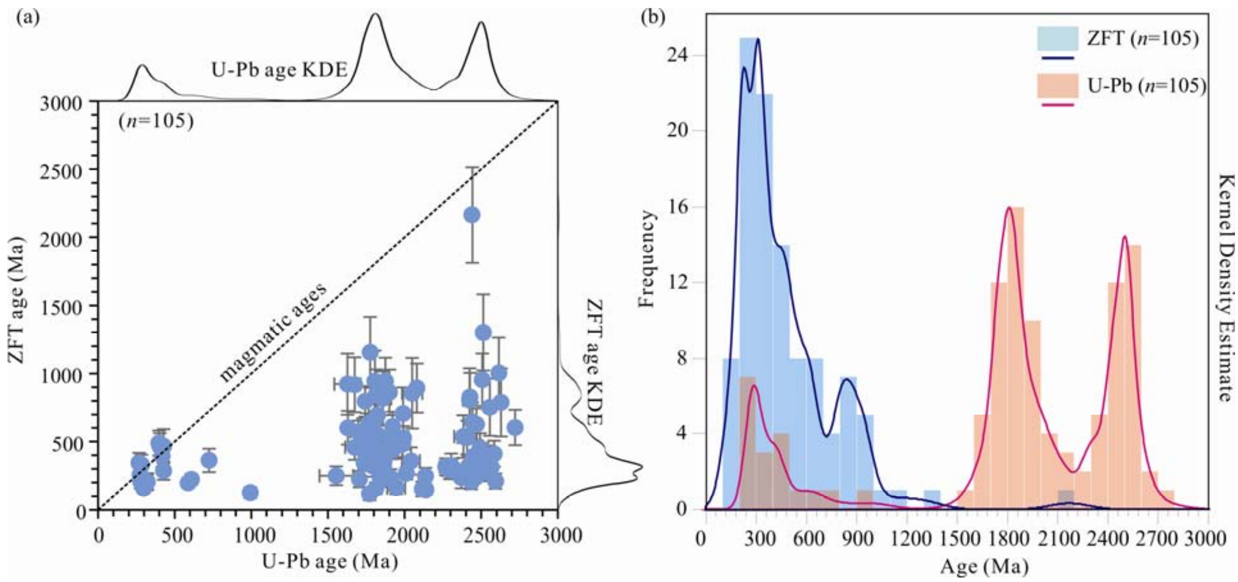

Fig. 5. (a) Fission-track versus U-Pb ages for double-dated zircon grains for the whole data set, and corresponding fission-track and U-Pb age kernel density estimate (KDE); (b) histograms and kernel density estimates of detrital zircon fission-track and U-Pb for the whole data set.

2012; Zhai, 2014). The Early Paleozoic U-Pb age population with the peak at 455.3±1.2 Ma (8.6±2.7%) matches the timing of the Early Paleozoic magmatic-metamorphic events in Qinling Orogenic Collage (Dong et al., 2011; Bader et al., 2013). The Early Permian U-Pb age population with the peak at 290.68±0.78 Ma (8.6±2.7%) coincides with coeval magmatism in the northern margin of the NCC (Wang et al., 2017). To sum up, detrital zircon U-Pb data indicate that the crystalline basement of the NCC is the primary provenance of the Permian-Middle Triassic sediments in the southern Ordos Basin, while the Permian magmatites in the northern margin of the NCC and Early Paleozoic crystalline rocks in Qinling Orogenic Collage act as minor provenance.

In general, detrital ZFT age populations may be younger, older, or equal to the depositional age of the sample within error. Detrital ZFT age populations that are younger than the depositional age of the sample indicate full or partial FT annealing after deposition, while an unreset sample is characterized by detrital ZFT age populations predating deposition (Bernet and Garver, 2005). Therefore, the unreset detrital ZFT age populations after deposition could be related to tectonothermal events in the source terrains and thus can be used as a tool for provenance analysis (Bernet and Garver, 2005; Falkowski et al., 2014).

As stated in Section 4.1, all samples in this study contain multiple age components and we have decomposed the mix ages into several distinct age populations (Table 3). Except Samples WB2, WB5, and WB6 have a youngest age population P1 younger than their corresponding depositional age, other decomposed age populations are older or equal to the depositional ages of the samples within error and thus recorded exhumation history of the source terrains. The Permian detrital ZFT age population P2 correlates with the full spectrum of U-Pb age peaks, suggesting that all of the source terrains experienced a syn-depositional exhumation. The Late Devonian-early Late Carboniferous detrital ZFT age population P3 correspond to U-Pb age populations with peaks at 2532.9±2.6 Ma, 1997.5±3.8 Ma, 1767.9±3.5 Ma, and 455.3±1.2 Ma, reflecting that coeval exhumation of the crystalline basement of the NCC and coeval volcanism or rapid exhumation in Qinling Orogenic Collage. The Late Neoproterozoic detrital ZFT age population P4 correspond to U-Pb age populations with peaks at 2532.9±2.6 Ma, 1997.5±3.8 Ma, and 1767.9±3.5 Ma, implying that the coeval exhumation of the crystalline basement of the NCC. The Paleoproterozoic detrital ZFT age population P5 with a near identical U-Pb age population suggests that coeval volcanism or rapid exhumation of the NCC.

Lag time, defined as the difference between the cooling age and the depositional age for a detrital mineral (Garver and Brandon, 1994; Bernet and Garver, 2005; Reiners and Brandon, 2006), provides an estimate of the lag or difference for the sample between closure in the source area and deposition in the adjacent basin (Bernet and Garver, 2005). In this study, the prominent unrest detrital ZFT age populations have different lag times (Fig. 6) and then contain critical information related to the source-to-

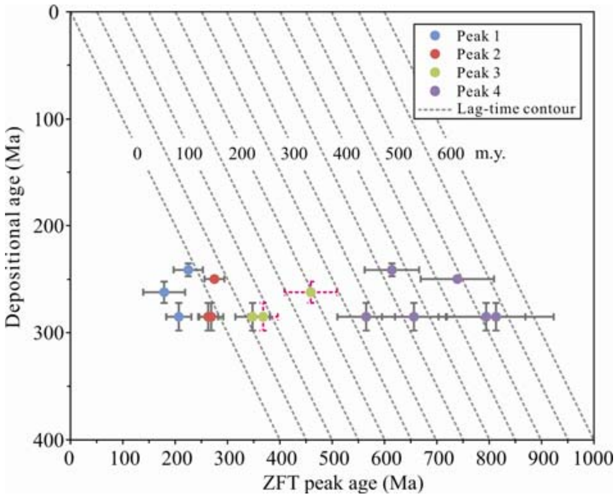

Fig. 6. Lag time plot of detrital zircon fission-track age peaks from the Permian-Middle Triassic sediments in the southern Ordos Basin.

sink processes of the Permian-Middle Triassic sediments in the southern Ordos Basin. Detailly, the unreset detrital ZFT age population P2 shows little variation upsection and falls into a lag-time interval ranging from 0 to 50 m.y. within error, suggesting that it is a static peak and recorded rapid cooling of the source terrains in the past. The detrital ZFT age population P3 falls into a lag-time interval at 50 m.y. within error, implying that these zircons were recycled from earlier sediments or experienced a very slow exhumation-erosion-deposition processes. The detrital ZFT age population P4 falls into a large and wide lag-time interval ranging from 250 to 600 m.y. within error. Bernet and Garver (2005) suggested that zircons with lag-time interval ranging 10–10^2 m.y. are typically recycled from sedimentary cover units. Thus, we suggest that these zircons consisting of the detrital ZFT age population P4 were mostly recycled from pre-Permian sediments that were ultimately sourced from the basement of the NCC.

5.2 Tectonic significance of the prominent ZFT peak age populations

As mentioned above, the decomposed ZFT ages of the Permian-Middle Triassic sediments in the southern Ordos Basin show four prominent peak age populations (Table 3) and thus record four major tectonothermal events (Fig. 7).

The Late Triassic-Early Jurassic ZFT age peak (P1) is obviously younger than the corresponding depositional age, indicating that these detrital zircons seemingly experienced the partial annealing owing to the post-depositional tectonothermal events. Previous thermal history study (Ren, 1996) suggested that the geothermal gradient of Ordos basin were relatively lower during Paleozoic-Early Mesozoic, ranging from 22–30 °C/km; while during Late Mesozoic the geothermal gradient began to increase and reached its peaks, and the geothermal gradient is 33–45 °C/km and the Upper Paleozoic-Lower Mesozoic rocks experienced a maximum paleo-temperature of approximately 200° C simultaneously. In this study, however, Samples WB2,

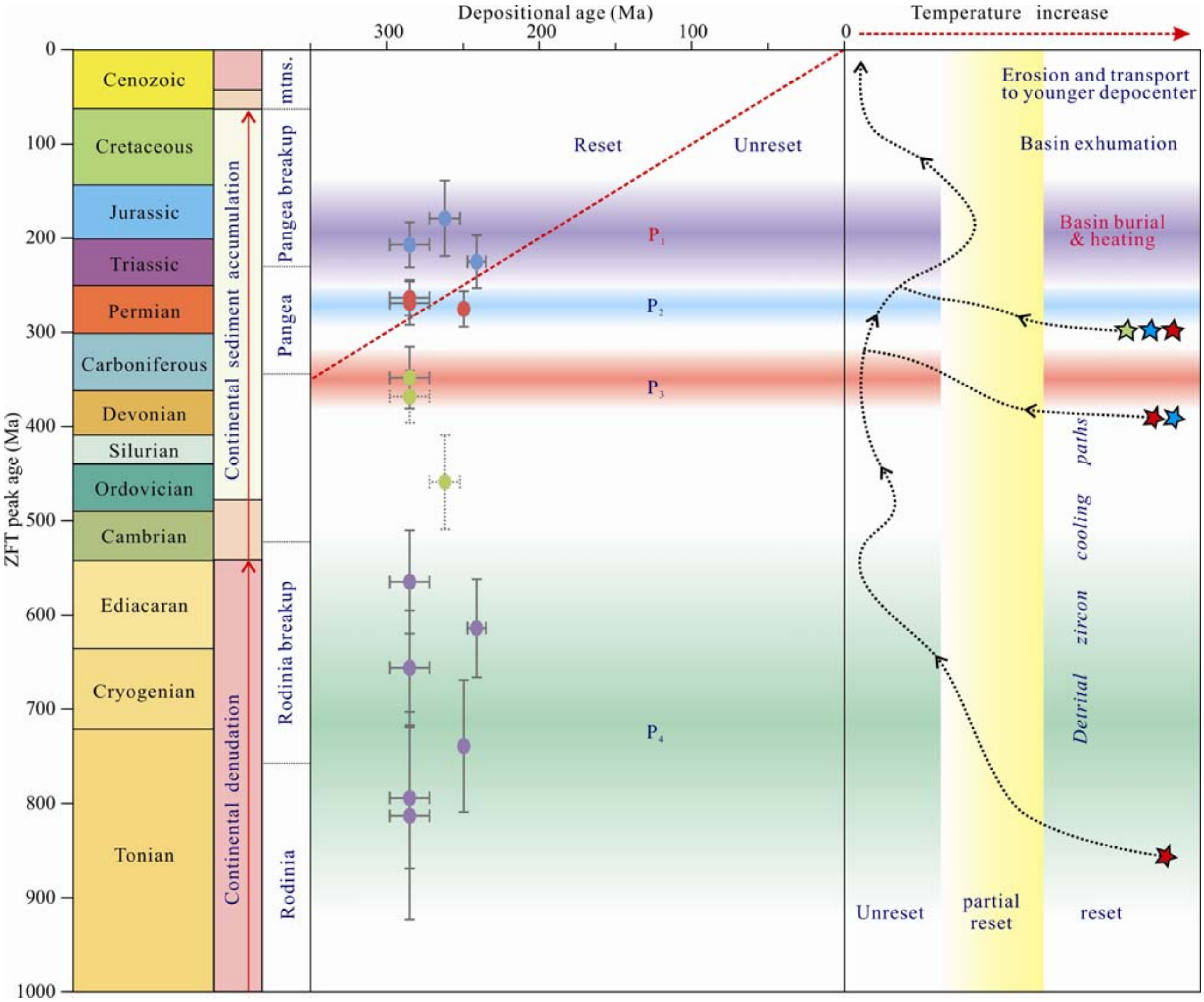

Fig.7. Schematic illustration of the major tectonothermal events (left) and provenance evolution (right) in the southern Ordos Basin. The red star represents zircon grains derived from the basement of the NCC; the blue star represents zircons grains derived from the Early Paleozoic crystalline rocks in Qinling Orogenic Collage; the yellow star represents zircons grains derived from the Permian magmatites in the northern margin of NCC.

WB5, and WB6 experienced a partial annealing, indicating that it was Late Triassic-Early Jurassic rather than Late Mesozoic that the southern Ordos Basin experienced a maximum paleo-temperature and the maximum paleo-temperature was 210–300°C. Although the Late Triassic-Early Jurassic tectonothermal event in Ordos Basin has not been reported, it is believed that this tectonothermal event did occur and might only be distributed in the southwestern Ordos Basin. The reasons for this inference are as follows: 1) the partial annealed samples are just distributed in the southwestern Ordos Basin; 2) recent drilling discovered Late Triassic igneous rocks in the southwestern Ordos Basin; 3) 2D seismic interpretation found Late Triassic igneous intrusions; and 4) geochemical study suggested that the Late Triassic Yanchang Formation in the southwestern Ordos Basin received significant magmatic-hydrothermal input during deposition (He et al., 2016). Putting all these together, it is evident that during Late Triassic the southwestern Ordos Basin experienced a significant tectonothermal event, characterized by intense deep activity and thermal abnormality. Moreover, we suggest that this tectonothermal event was closely related to the coeval northward subduction of the Yangze Block and the following collision of the Yangze Block and the NCC (Meng and Zhang, 1999; Dong et al., 2011), which inducing the upwelling of deep material and energy beneath the southwestern Ordos Basin.

As mentioned in Section 4.1 and 5.1, the unrest Mid-Late Permian ZFT age peak (P2) overlaps the corresponding depositional ages for these samples within error, or is slightly older, and correlates with the full spectrum of U-Pb age peaks, suggesting that syn-depositional volcanic input or all of the source terrains experienced a rapid exhumation. In fact, the northern part of the NCC experienced multiple exhumation episodes and magmatic activities during Middle Permian-Triassic, which have a close relationship with the southward subduction of the Paleo-Asian Ocean beneath the NCC and subsequent collision (Ma et al., 2014; Wang et al., 2017). Moreover, the North Qinling terrane, a major tectonic unit of Qinling Orogenic Collage, experienced a compression-related uplift event during Mid-Late Permian, which probably a response to northward subduction of the Paleo-Tethyan Ocean and South Qinling (Yang et al., 2017). Consequently, we interpreted the unrest Mid-Late Permian ZFT age peak recorded coeval denudation in the northern part of the NCC and North Qinling terrane.

The Late Devonian-early Late Carboniferous tectonothermal event was definitely revealed by ZFT age peak P3 of the Sample WB7 (348±33 Ma, 53% of dated grains). In addition, Samples WB5 and WB6 also contain ZFT age peak P3, while the geological meaning is vague owing to the partial annealing after deposition. Notably, the NCC experienced a long-term denudation during the Late Ordovician-Early Carboniferous (Yang et al., 2005). Meanwhile, North Qinling terrane and the southern NCC experienced a significant tectonothermal event because of the northward subduction and closure of the Shangdan Ocean along the southern edge of the NCC (Meng and Zhang, 2000). The northern NCC also experienced a coeval tectonothermal event due to the accretion of the Bainaimiao arc to the northern NCC during the Late Silurian-earliest Devonian by arc-continent collision (Zhang et al., 2014). Therefore, we suggested that the Late Devonian-early Late Carboniferous ZFT age peak recorded coeval denudation in the hinterland and periphery of the NCC.

The Late Neoproterozoic ZFT age peak (P4) is also markedly older than the corresponding depositional ages and correlates with the U-Pb age spectrum of the crystalline basement of the NCC, implying that these zircon grains were probably recycled from pre-Permian sediments that were ultimately sourced from the basement of the NCC and experienced a long term denudation during Late Neoproterozoic. In fact, the Late Neoproterozoic denudation has been widely recognized worldwide, characterized by the Great Unconformity, a global erosion surface separating Precambrian and Paleozoic rocks, representing ~100–1000 m.y. of missing geologic time (Peters and Gaines, 2012; He et al., 2017; DeLucia et al., 2018). Erosion that formed the Great Unconformity has been causally linked to Rodinia breakup, Snowball Earth, and the Cambrian explosion (Peters and Gaines, 2012; Cox et al., 2016; He et al., 2016; DeLucia et al., 2018). Nevertheless, the timing and duration of denudation associated with formation of the Great Unconformity remain uncertain (He et al., 2017; DeLucia et al., 2018). Here, we propose that the ZFT age peak P4, ranging from ca. 813 Ma to ca. 565 Ma, provides a constraint on the timing of the Late Neoproterozoic denudation within the NCC. This inference is supported by a chronostratigraphic study based on detrital zircon age data (He et al., 2017), which suggested that the NCC experienced a depositional hiatus of >150–300 m.y. during Tonian to Ediacaran. In addition, recent palaeogeographical reconstruction (Li et al., 2013) suggested that the NCC was situated in a divergent tectonic setting during Late Neoproterozoic, which rules out mechanism of coeval denudation that result solely from convergent tectonics. Instead, numerous Neoproterozoic mafic dykes have been recognized within the NCC, implying that an upwelling mantle plume possibly existed during Neoproterozoic (Peng et al., 2011; Wang et al., 2016). Moreover, our documented timing of the Late Neoproterozoic denudation within the NCC overlaps with the timing of Rodinia breakup (Gernon et al., 2016). Therefore, we interpret the Late Neoproterozoic denudation as a result of a large-scale mantle upwelling following Rodinia supercontinent assembly because of a large-scale mantle upwelling that can simultaneously explain uplift in the continental interior and rifting at the margins (Zhang et al., 2012; DeLucia et al., 2018).

6 Conclusions

This study presents detrital zircon fission-track and U-Pb double analyses of the Permian to Middle Triassic sediments in the southern Ordos Basin to decipher the tectonic information archived in the sediments of intracratonic basins, and thus provides constraints on provenance evolution and regional tectono-thermal events. From our study the following conclusions can be drawn:

The Permian-Middle Triassic sediments in the southern Ordos Basin were sourced from multiple provenance, and the crystalline basement of the NCC and recycled materials from pre-Permian sediments that were ultimately sourced from the basement of the NCC are the primary provenance, while the Permian magmatites in the northern margin of NCC and Early Paleozoic crystalline rocks in Qinling Orogenic Collage act as minor provenance.

The Permian-Middle Triassic sediments in the southern Ordos Basin recorded four major tectonothermal events, including the Late Triassic-Early Jurassic post-depositional tectonothermal event and three other tectonothermal events associated with source terrains. The Late Triassic-Early Jurassic tectonothermal event was closely related to the upwelling of deep material and energy beneath the southwestern Ordos Basin due to the coeval northward subduction of the Yangze Block and the following collision of the Yangze Block and the NCC. The Mid-Late Permian tectonothermal event was connected with coeval denudation in the northern part of the NCC and North Qinling terrane, resulting from the subduction of the Paleo-Asian Ocean and Tethys Ocean toward the NCC, respectively. The Late Devonian-early Late Carboniferous tectonothermal event corresponded the long-term denudation in the hinterland and periphery of the NCC because of the arc-continent collisions in the northern and southern margins of the NCC. The Late Neoproterozoic tectonothermal event was associated with formation of the Great Unconformity within the NCC and may be causally related to the Rodinia supercontinent breakup driven by a large-scale mantle upwelling.

Acknowledgements

LI Yiwei and JIA Chunyang are acknowledged for sampling assistance in the field. Zircon fission-track and U-Pb double dating were accomplished by Dr. Cleber J. SOARES at ChronusCamp Research Thermochronology

Laboratory, Brazil. We thank the anonymous reviewer and the Editor for their comments and suggestions, which significantly improved the quality of the manuscript. This work was supported by the National Natural Science Foundation of China (Grants No. 41572102, 41330315, 41102067, and 41172127) and and Natural Science Foundation of Shaanxi Province (Grant No. 2018JM4001).

Manuscript received Mar. 10, 2018
accepted May 17, 2018
associate EIC YANG Jingsui
edited by FEI Hongcai

References

Allen, P.A., and Armitage, J.J., 2012. Cratonic Basins, in: Tectonics of Sedimentary Basins. John Wiley & Sons, Ltd, Chichester, UK: 602–620.

Bader, T., Franz, L., Ratschbacher, L., de Capitani, C., Webb, A.A.G., Yang, Z., Pfänder, J.A., Hofmann, M., and Linnemann, U., 2013. The Heart of China revisited: II Early Paleozoic (ultra) high-pressure and (ultra) high-temperature metamorphic Qinling orogenic collage. Tectonics, 32(4): 922–947.

Bai, Y., Ma, Y., Huang, Y., Liao, J., and Liu, X., 2013. Properties of continental margin and its hydrocarbon exploration significance in Cambrian in the Southern Ordos Kratogen of North China. Acta Geologica Sinica (English Edition), 88(3): 777–803.

Bernet, M., and Garver, J. I., 2005. Fission-track Analysis of Detrital Zircon. Reviews in Mineralogy and Geochemistry, 58: 205–237.

Bernet, M., van der Beek, P., Pik, R., Huyghe, P., Mugnier, J.-L., Labrin, E., and Szulc, A., 2006. Miocene to Recent exhumation of the central Himalaya determined from combined detrital zircon fission-track and U-Pb analysis of Siwalik sediments, western Nepal. Basin Research, 18: 393–412.

Brandon, M.T., 1992. Decomposition of fission-track grain-age distributions. American Journal of Science, 292: 535–564.

Cao, K., Wang, G.C., Bernet, M., van der Beek, P., and Zhang, K.X., 2015. Exhumation history of the West Kunlun Mountains, northwestern Tibet: Evidence for a long-lived, rejuvenated orogen. Earth and Planetary Science Letters, 432: 391–403.

Carrapa, B., 2010. Resolving tectonic problems by dating detrital minerals. Geology, 38: 191–192.

Carter, A., and Bristow, C.S., 2000. Detrital zircon geochronology: Enhancing the quality of sedimentary source information through improved methodology and combined U-Pb and fission-track techniques. Basin Research, 12: 47–57.

Carter, A., and Moss, S.J., 1999. Combined detrital-zircon fission-track and U-Pb dating: A new approach to understanding hinterland evolution. Geology, 27: 235–238.

Cawood, P.A., Hawkesworth, C.J., and Dhuime, B., 2012. Detrital zircon record and tectonic setting. Geology, 40: 875–878.

Cawood, P.A., Nemchin, A.A., Strachan, R., Prave, T., and Krabbendam, M., 2007. Sedimentary basin and detrital zircon record along East Laurentia and Baltica during assembly and breakup of Rodinia. Journal of the Geological Society, 164: 257–275.

Chen, Y., Fu, J., Yang, G., Xiao, A., Sun, L., Xu, B., Bao, H., and Mao, L., 2016. Researches on basin property of Ordos block during Mesoproterozoic Changcheng Period. Acta Petrologica Sinica, 32(3): 856–864 (in Chinese with English abstract).

Cheng, X., Lin, X., Wu, L., Chen, H., Xiao, A., Gong, J., Zhang, F., and Yang, S., 2016. The Exhumation History of North Qaidam Thrust Belt Constrained by Apatite Fission Track Thermochronology: Implication for the Evolution of the Tibetan Plateau. Acta Geologica Sinica (English Edition), 90 (3): 870–883.

Curvo, E.A.C., Tello S., C.A., Carter, A., Dias, A.N.C., Soares, C.J., Nakasuga, W.M., Resende, R.S., Gomes, M.R., Alencar, I., and Hadler, J.C., 2013. Zircon fission track and U-Pb dating methods applied to São Paulo and Taubaté Basins located in the southeast Brazil. Radiation Measurements, 50: 172–180.

Darby, B.J., and Ritts, B.D., 2002. Mesozoic contractional deformation in the middle of the Asian tectonic collage: The intraplate Western Ordos fold-thrust belt, China. Earth and Planetary Science Letters, 205: 13–24.

De Grave, J., Zhimulev, F.I., Glorie, S., Kuznetsov, G.V., Evans, N., Vanhaecke, F., and McInnes, B., 2016. Late Palaeogene emplacement and late Neogene-Quaternary exhumation of the Kuril island-arc root (Kunashir island) constrained by multi-method thermochronometry. Geoscience Frontiers, 7: 211–220.

DeLucia, M.S., Guenthner, W.R., Marshak, S., Thomson, S.N., and Ault, A.K., 2018. Thermochronology links denudation of the Great Unconformity surface to the supercontinent cycle and snowball Earth. Geology, 46(2): 167–170.

Dias, A.N.C., Chemale, F., Hackspacher, P.C., Soares, C.J., O-Aristizabal, C.I., and Tello, C.A.S., 2018. Fission track and U-Pb double dating of detrital zircon applied to the intracratonic Mesozoic Bauru Basin, Brazil. Geological Journal, 53(5): 1767–1780.

Dias, A.N.C., Tello, C.A.S., Chemale, F., de Godoy, M.C.T.F., Guadagnin, F., Iunes, P.J., Soares, C.J., Osório, A.M.A., and Bruckmann, M.P., 2011. Fission track and U-Pb in situ dating applied to detrital zircon from the Vale do Rio do Peixe Formation, Bauru Group, Brazil. Journal of South American Earth Sciences, 31: 298–305.

Dickinson, W.R., and Gehrels, G.E., 2009. Use of U-Pb ages of detrital zircons to infer maximum depositional ages of strata: A test against a Colorado Plateau Mesozoic database. Earth and Planetary Science Letters, 288: 115–125.

Donelick, R.A., O'Sullivan, P.B., and Ketcham, R.A., 2005. Apatite Fission-Track Analysis. Reviews in Mineralogy & Geochemistry, 58: 49–94.

Dong, Y., Zhang, G., Neubauer, F., Liu, X., Genser, J., and Hauzenberger, C., 2011. Tectonic evolution of the Qinling orogen, China: Review and synthesis. Journal of Asian Earth Sciences, 41: 213–237.

Fedo, C.M., Sircombe, K.N., and Rainbird, R.H., 2003. Detrital zircon analysis of the sedimentary record. Reviews in Mineralogy & Geochemistry, 53: 277–303.

Filleaudeau, P.Y., Mouthereau, F., and Pik, R., 2012. Thermo-tectonic evolution of the south-central Pyrenees from rifting to orogeny: Insights from detrital zircon U-Pb and (U-Th)/He thermochronometry. Basin Research, 24: 401–417.

Fosdick, J.C., Grove, M., Graham, S.A., Hourigan, J.K., Lovera, O., and Romans, B.W., 2015. Detrital thermochronologic record of burial heating and sediment recycling in the Magallanes foreland basin, Patagonian Andes. Basin Research, 27: 546–572.

Galbraith, R.F., 1981. On statistical models for fission track counts. Journal of the International Association for Mathematical Geology, 13: 471–478.

Galbraith, R.F., 1984. On statistical estimation in fission track dating. Journal of the International Association for Mathematical Geology, 16: 653–669.

Gallagher, K., Brown, R., and Johnson, C., 1998. Fission track analysis and its applications to geological problems. Annual Review of Earth and Planetary Sciences, 26: 519–572.

Garver, J.I., and Brandon, M.T., 1994. Erosional denudation of the British Columbia Coast Ranges as determined from fission -track ages of detrital zircon from the Tofino basin, Olympic Peninsula, Washington. Geological Society of America Bulletin, 106: 1398–1412.

Gehrels, G., 2014. Detrital Zircon U-Pb Geochronology Applied to Tectonics. Annual Review of Earth and Planetary Sciences, 42: 127–149.

Gernon, T.M., Hincks, T.K., Tyrrell, T., Rohling, E.J., and Palmer, M.R., 2016. Snowball Earth ocean chemistry driven by extensive ridge volcanism during Rodinia breakup. Nature

Geoscience, 9: 242–248.
Giorgis, S., Weber, J., Sanguinito, S., Beno, C., and Metcalf, J., 2017. Thermochronology constraints on miocene exhumation in the central range mountains, Trinidad. Geological Society of America Bulletin, 129: 171–178.
Glorie, S., Alexandrov, I., Nixon, A., Jepson, G., Gillespie, J., and Jahn, B.M., 2017. Thermal and exhumation history of Sakhalin Island (Russia) constrained by apatite U-Pb and fission track thermochronology. Journal of Asian Earth Sciences, 143: 326–342.
Glorie, S., and De Grave, J., 2016. Exhuming the Meso-Cenozoic Kyrgyz Tianshan and Siberian Altai-Sayan: A review based on low-temperature thermochronology. Geoscience Frontiers, 7: 155–170.
Gong, W., Xi, S., Liu, X., Hu, J., and Li, Z., 2016. LA-ICP-MS U-Pb dating of detrital zircons from Changcheng System in Ordos Block,Western North China Craton and its implications. Geological Review, 62(6): 1379–1391 (in Chinese with English abstract).
Guadagnin, F., Chemale Junior, F., Magalhães, A.J.C., Alessandretti, L., Bállico, M.B., and Jelinek, A.R., 2015. Sedimentary petrology and detrital zircon U-Pb and Lu-Hf constraints of Mesoproterozoic intracratonic sequences in the Espinhaço Supergroup: Implications for the Archean and Proterozoic evolution of the São Francisco Craton. Precambrian Research, 266: 227–245.
Guo, Z., Peng, S., Hao, Q., Biscaye, P.E., An, Z., and Liu, T., 2004. Late Miocene–Pliocene development of Asian aridification as recorded in the Red-Earth Formation in northern China. Global and Planetary Change, 41: 135–145.
Hasebe, N., Barbarand, J., Jarvis, K., Carter, A., and Hurford, A.J., 2004. Apatite fission-track chronometry using laser ablation ICP-MS. Chemical Geology, 207: 135–145.
He, C., Ji, L., Wu, Y., Su, A., and Zhang, M., 2016. Characteristics of hydrothermal sedimentation process in the Yanchang Formation, south Ordos Basin, China: Evidence from element geochemistry. Sedimentary Geology, 345: 33–41.
He, T., Zhou, Y., Vermeesch, P., Rittner, M., Miao, L., Zhu, M., Carter, A., Pogge von Strandmann, P.A.E., and Shields, G.A., 2017. Measuring the "Great Unconformity" on the North China Craton using new detrital zircon age data. Geological Society, London, Special Publications, 448: 145–159.
Hietpas, J., Samson, S., Moecher, D., and Schmitt, A.K., 2010. Recovering tectonic events from the sedimentary record: Detrital monazite plays in high fidelity. Geology, 38: 167–170.
Hodges, K. V., Ruhl, K. W., Wobus, C. W., and Pringle, M. S., 2005. $^{40}Ar/^{39}Ar$ Thermochronology of detrital minerals. Reviews in Mineralogy & Geochemistry, 58: 239–257.
Hoskin, P.W.O., and Black, L.P., 2000. Metamorphic zircon formation by solid-state recrystallization of protolith igneous zircon. Journal of Metamorphic Geology, 18: 423–439.
Ketcham, R.A., Donelick, R.A., and Donelick, M.B., 2003. AFTSolve: A program for multi-kinetic modeling of apatite fission-track data. American Mineralogist, 88: 929.
Klein, G. de V, and Hsui, A.T., 1987. Origin of cratonic basins. Geology, 15: 1094–1098.
Kounov, A., Viola, G., Dunkl, I., and Frimmel, H.E., 2013. Southern African perspectives on the long-term morpho-tectonic evolution of cratonic interiors. Tectonophysics, 601: 177–191.
Kusky, T.M., Windley, B.F., and Zhai, M.-G., 2007. Tectonic evolution of the North China Block: from orogen to craton to orogen. Geological Society, London, Special Publications, 280: 1–34.
Lawton, T.F., 2014. Small grains, big rivers, continental concepts. Geology, 42: 639–640.
Li, R., and Li, Y., 2008. Tectonic evolution of the western margin of the Ordos Basin (Central China). Russian Geology and Geophysics, 49: 23–27.
Li, Z.-X., Evans, D.A.D., and Halverson, G.P., 2013. Neoproterozoic glaciations in a revised global palaeogeography from the breakup of Rodinia to the assembly of Gondwanaland. Sedimentary Geology, 294: 219–232.
Liu, C., Liu, F., and Zhao, G., 2012. Paleoproterozoic basin evolution in the Trans-North China Orogen, North China Craton. Acta Petrologica Sinica, 28(9): 2770–2784 (in Chinese with English abstract).
Liu, C., Zhao, H., Zhao, J., Wang, J., Zhang, D., and Yang, M., 2008. Temporo-spatial coordinates of evolution of the Ordos basin and its mineralization responses. Acta Geologica Sinica (English Edition), 82(6): 1229–1243.
Lu, S., Zhao, G., Wang, H., and Hao, G., 2008. Precambrian metamorphic basement and sedimentary cover of the North China Craton: A review. Precambrian Research, 160: 77–93.
Ma, S., Meng, Q., Duan, L., and Wu, G., 2014. Reconstructing Late Paleozoic exhumation history of the Inner Mongolia Highland along the northern edge of the North China Craton. Journal of Asian Earth Sciences, 87: 89–101.
Mark, C., Cogné, N., and Chew, D., 2016. Tracking exhumation and drainage divide migration of the Western Alps: A test of the apatite U-Pb thermochronometer as a detrital provenance tool. Geological Society of America Bulletin, 128: 1439–1460.
Meng, Q., 2017. Origin of the Qinling Mountains. Scientia Sinica Terrae, 47: 412–420 (in Chinese).
Meng, Q.R., and Zhang, G.W., 1999. Timing of collision of the North and South China blocks: Controversy and reconciliation. Geology, 27: 123–126.
Peng, P., Bleeker, W., Ernst, R.E., Söderlund, U., and McNicoll, V., 2011. U-Pb baddeleyite ages, distribution and geochemistry of 925Ma mafic dykes and 900Ma sills in the North China craton: Evidence for a Neoproterozoic mantle plume. Lithos, 127: 210–221.
Peters, S.E., and Gaines, R.R., 2012. Formation of the 'Great Unconformity' as a trigger for the Cambrian explosion. Nature, 484: 363–366.
Pinet, N., Lavoie, D., Dietrich, J., Hu, K., and Keating, P., 2013. Architecture and subsidence history of the intracratonic Hudson Bay Basin, northern Canada. Earth-Science Reviews, 125: 1–23.
Reiners, P.W., and Brandon, M.T., 2006. Using thermochronology to understand orogenic erosion. Annual Review of Earth and Planetary Sciences, 34: 419–466.
Reiners, P.W., Campbell, I.H., Nicolescu, S., Allen, C.M., Hourigan, J.K., Garver, J.I., Mattinson, J.M., and Cowan, D.S., 2005. (U-Th)/(He-Pb) double dating of detrital zircons. American Journal of Science, 305: 259–311.
Ren, Z., 1996. Research on the relations between geothermal history and oil-gas accumulation in the Ordos Basin. Acta Petrolei Sinica, 17: 17–24 (in Chinese with English abstract).
Shen, C.B., Donelick, R.A., O'Sullivan, P.B., Jonckheere, R., Yang, Z., She, Z.B., Miu, X.L., and Ge, X., 2012. Provenance and hinterland exhumation from LA-ICP-MS zircon U-Pb and fission-track double dating of Cretaceous sediments in the Jianghan Basin, Yangtze block, central China. Sedimentary Geology, 281: 194–207.
Shen, T., Wang, G., Leloup, P.H., van der Beek, P., Bernet, M., Cao, K., Wang, A., Liu, C., and Zhang, K., 2016. Controls on Cenozoic exhumation of the Tethyan Himalaya from fission-track thermochronology and detrital zircon U-Pb geochronology in the Gyirong basin area, southern Tibet. Tectonics, 35: 1713–1734.
Soares, C.J., Guedes, S., Hadler, J.C., Mertz-Kraus, R., Zack, T., and Iunes, P.J., 2014. Novel calibration for LA-ICP-MS-based fission-track thermochronology. Physics and Chemistry of Minerals, 41: 65–73.
Stuart, F.M., Bluck, B.J., and Pringle, M.S., 2001. Detrial muscovite $^{40}Ar/^{39}Ar$ ages from Carboniferous sandstones of the British Isles: Provenance and implications for th uplift history of orogenic belts. Tectonics, 20: 255–267.
Sun, Y., Lu, H., and An, Z., 2006. Grain size of loess, palaeosol and Red Clay deposits on the Chinese Loess Plateau: Significance for understanding pedogenic alteration and palaeomonsoon evolution. Palaeogeography, Palaeoclimatology, Palaeoecology, 241: 129–138.
Thomas, W.A., 2011. Detrital-zircon geochronology and sedimentary provenance. Lithosphere, 3: 304–308.
Thomson, K.D., Stockli, D.F., Clark, J.D., Puigdefàbregas, C.,

and Fildani, A., 2017. Detrital zircon (U-Th)/(He-Pb) double-dating constraints on provenance and foreland basin evolution of the Ainsa Basin, south-central Pyrenees, Spain. Tectonics, 36: 1352–1375.

Vermeesch, P., 2004. How many grains are needed for a provenance study? Earth and Planetary Science Letters, 224: 441–451.

Vermeesch, P., 2009. RadialPlotter: A Java application for fission track, luminescence and other radial plots. Radiation Measurements, 44: 409–410.

Wang, C., Dai, J., Zhao, X., Li, Y., Graham, S.A., He, D., Ran, B., and Meng, J., 2014. Outward-growth of the Tibetan Plateau during the Cenozoic: A review. Tectonophysics, 621: 1–43.

Wang, C., Peng, P., Wang, X., and Yang, S., 2016. Nature of three Proterozoic (1680 Ma, 1230 Ma and 775 Ma) mafic dyke swarms in North China: Implications for tectonic evolution and paleogeographic reconstruction. Precambrian Research, 285: 109–126.

Wang, Q., Deng, J., Huang, D., Yang, L., Gao, B., Xu, H. and Jiang, S., 2006. Tectonic constraints on the transformation of Paleozoic framework of uplift and depression in the Ordos area. Acta Geologica Sinica (English Edition), 80(6): 944–953.

Wang, T., Tong, Y., Zhang, L., Li, S., Huang, H., Zhang, J., Guo, L., Yang, Q., Hong, D., Donskaya, T., Gladkochub, D., and Tserendash, N., 2017. Phanerozoic granitoids in the central and eastern parts of Central Asia and their tectonic significance. Journal of Asian Earth Sciences, 145: 368–392.

Xu, J., Stockli, D.F., and Snedden, J.W., 2017. Enhanced provenance interpretation using combined U–Pb and (U–Th)/He double dating of detrital zircon grains from lower Miocene strata, proximal Gulf of Mexico Basin, North America. Earth and Planetary Science Letters, 475: 44–57.

Yang, D.-B., Yang, H.-T., Shi, J.-P., Xu, W.-L., and Wang, F., 2017. Sedimentary response to the paleogeographic and tectonic evolution of the southern North China Craton during the late Paleozoic and Mesozoic. Gondwana Research, 49: 278–295.

Yang, M., Li, L., Zhou, J., Jia, H., Sun, X., Gong, T., and Ding, C., 2015. Structural evolution and hydrocarbon potential of the upper Paleozoic northern Ordos basin, north China. Acta Geologica Sinica (English Edition), 89(5): 1636–1648.

Yang, Y., Li, W., and Ma, L., 2005. Tectonic and stratigraphic controls of hydrocarbon systems in the Ordos basin: A multicycle cratonic basin in central China. AAPG Bulletin, 89: 255–269.

Zhai, M., 2011. Cratonization and the Ancient North China Continent: A summary and review. Science China Earth Sciences, 54(8): 1110–1120.

Zhai, M., 2014. Multi-stage crustal growth and cratonization of the North China Craton. Geoscience Frontiers, 5: 457–469.

Zhai, M., and Liu, W., 2003. Palaeoproterozoic tectonic history of the North China craton: A review. Precambrian Research, 122: 183–199.

Zhai, M., Hu, B., Zhao, T., Peng, P., and Meng, Q., 2014. Late Paleoproterozoic-Neoproterozoic multi-rifting events in the North China Craton and their geological significance: A study advance and review. Tectonophysics, 662: 153–166.

Zhang, N., Zhong, S., and Flowers, R.M., 2012. Predicting and testing continental vertical motion histories since the Paleozoic. Earth and Planetary Science Letters, 317–318: 426–435.

Zhang, S., Liu, C., Yang, M., Bai, J., and WANG, J., 2018b. Latest Triassic to Early Jurassic thrusting and exhumation in the Southern Ordos Basin, North China: Evidence from LA–ICP–MS–based apatite fission track thermochronology. Acta Geologica Sinica (English Edition), 92(4): 1334–1348.

Zhang, S., Wang, J., Liu, C., Bai, J., Peng, H., Huang, H., and Guan, Y., 2018a. Detrital zircon U–Pb geochronology of the Permian strata in the Turpan–Hami Basin in North Xinjiang, NW China: Depositional age, provenance, and tectonic implications. Geological Journal (in press). Doi: 10.1002/gj.3374.

Zhang, S.H., Zhao, Y., Ye, H., Liu, J.M., and Hu, Z.C., 2014. Origin and evolution of the Bainaimiao arc belt: Implications for crustal growth in the southern Central Asian orogenic belt. Geological Society of America Bulletin, 126: 1275–1300.

Zhang, Y., Shi, W., and Dong, S., 2011. Changes of Late Mesozoic Tectonic Regimes around the Ordos Basin (North China) and their Geodynamic Implications. Acta Geologica Sinica (English Edition), 85(6): 1254–1276.

Zhao, G., Cawood, P.A., Li, S., Wilde, S.A., Sun, M., Zhang, J., He, Y., and Yin, C., 2012. Amalgamation of the North China Craton: Key issues and discussion. Precambrian Research, 222–223: 55–76.

Zhao, G., Wilde, S.A., Cawood, P.A., and Sun, M., 2001. Archean blocks and their boundaries in the North China Craton: Lithological, geochemical, structural and P-T path constraints and tectonic evolution. Precambrian Research, 107: 45–73.

Zhao, J., Liu, C., Wang, X., and Zhang, C., 2009. Migration of depocenters and accumulation centers and its indication of subsidence centers in the Mesozoic Ordos Basin. Acta Geologica Sinica (English Edition), 83(2): 278–294.

Zhao, X., Liu, C., Wang, J., Zhao, Y., Zhang, D., Wang, L., Deng, Y., and Guo, P., 2016. Mesozoic–Cenozoic tectonic uplift events of Xiangshan Mountain in northern North-South Tectonic Belt, China. Acta Petrologica Sinica, 32(7): 2124–2136 (in Chinese with English abstract).

Zhu, H., Liu, K., Yang, X., and Liu, Q., 2013. Sedimentary controls on the sequence stratigraphic architecture in intra-cratonic basins: An example from the Lower Permian Shanxi Formation, Ordos Basin, northern China. Marine and Petroleum Geology, 45: 42–54.

About the first author

ZHANG Shaohua, male, born in 1990 in Baoji City, Shaanxi Province. He is now a Ph.D. candidate of Northwest University. His current research interests include basin analysis, regional tectonics, and petroleum geology. E-mail: zhangshh86@163.com.

About the corresponding author

LIU Chiyang, male, born in 1953 in Xi'an City, Shaanxi Province. He is currently a professor of geology at Northwest University (China). He received his B.Sc. and M.Sc. degrees from Northwest University (China). His academic research career spans almost 40 years in the fields of basin analysis and petroleum geology. E-mail: lcy@nwu.edu.cn.